A molecular brake, not a clutch, stops the *Rhodobacter sphaeroides* flagellar motor

Teuta Pilizota[a,1,2], Mostyn T. Brown[b,1], Mark C. Leake[a,c], Richard W. Branch[a], Richard M. Berry[a], and Judith P. Armitage[b,c,3]

[a]The Clarendon Laboratory, Department of Physics, Oxford University, Parks Road, Oxford OX1 3PU, United Kingdom; [b]Department of Biochemistry, University of Oxford, South Parks Road, Oxford OX1 3QU, United Kingdom; and [c]Oxford Centre for Integrative Systems Biology (OCISB), Department of Biochemistry, University of Oxford, South Parks Road, Oxford OX1 3QU, United Kingdom

Many bacterial species swim by employing ion-driven molecular motors that power the rotation of helical filaments. Signals are transmitted to the motor from the external environment via the chemotaxis pathway. In bidirectional motors, the binding of phosphorylated CheY (CheY-P) to the motor is presumed to instigate conformational changes that result in a different rotor-stator interface, resulting in rotation in the alternative direction. Controlling when this switch occurs enables bacteria to accumulate in areas favorable for their survival. Unlike most species that swim with bidirectional motors, *Rhodobacter sphaeroides* employs a single stop-start flagellar motor. Here, we asked, how does the binding of CheY-P stop the motor in *R. sphaeroides*—using a clutch or a brake? By applying external force with viscous flow or optical tweezers, we show that the *R. sphaeroides* motor is stopped using a brake. The motor stops at 27–28 discrete angles, locked in place by a relatively high torque, approximately 2–3 times its stall torque.

Controlling the output of molecular motors is critical for many cellular processes governing cell growth, division, and transport. In addition, regulating their force-generating capabilities is a prerequisite for the operation of useful bionanodevices (1). Here, by examining the mechanics required to control the *Rhodobacter sphaeroides* flagellar motor, we provide an example of how molecular machines are controlled at the nanoscale.

The bacterial flagellar motor [reviewed in ref. 2 and 3] is a molecular machine made from several hundred proteins embedded in the cell envelope. It drives the rotation of an extracellular helical filament, enabling bacteria such as *Escherichia coli* to swim. The motor is powered by the cell's ion-motive force, usually maintained by electron transport (respiration/photosynthesis). The flow of ions through peptidoglycan-bound stator complexes, down an electrochemical gradient into the cytoplasm, is responsible for rotor rotation via electrostatic interactions at the rotor-stator interface (4). Stator units can independently engage/disengage from the rotor (5), resulting in stepwise changes in speed (6).

By controlling the output of the motor, *E. coli* can accumulate in areas favorable for their survival (7, 8). External conditions are sensed and transmitted via the chemotaxis pathway to the motor. This simple pathway controls the intracellular concentration of phosphorylated-CheY (CheY-P). In the absence of positive stimuli, CheY-P molecules bind to the rotor switch complex, which consists of approximately 26 copies of FliG, approximately 34 copies of FliM, and approximately 100 copies of FliN. Elevated CheY-P levels increase the probability that a change in direction of motor rotation occurs (9), causing a free-swimming bacterium to tumble (10). When motor rotation in its original direction recommences, the cell swims on a new trajectory. By controlling the frequency of motor switches, delaying tumbles when swimming up attractant gradients, cells achieve a biased random walk.

Many other bacterial species, such as the metabolically diverse α-proteobacterium *R. sphaeroides*, have more complicated chemosensory systems (reviewed in ref. 7). *R. sphaeroides* possesses multiple chemotaxis protein homologues, whose interactions are limited by differences in subcellular localization, expression level, and selective phosphotransfer (reviewed in ref. 11). A minimum of 2 CheY homologues can support chemotaxis in *R. sphaeroides*, $CheY_6$ plus either $CheY_3$ or $CheY_4$. Although $CheY_6$-P can stop the motor, it cannot mediate chemotaxis alone (12). Unlike *E. coli*, which has a switching motor, these CheYs control the behavior of a single unidirectional proton-driven flagellum termed fla1 (13). The cell is reoriented by relaxation of the flagellar filament from helical to coiled form when the motor stops (14).

Here, the mechanism used by the chemotaxis pathway to stop motor rotation was investigated. Data were obtained by either monitoring motor rotation at a high temporal and spatial resolution using back-focal-plane (BFP) interferometry or by manipulating motors using viscous flow or an optical trap.

We found that the motor rotates in the counterclockwise (CCW) direction at similar torques and speeds to *E. coli*, and that without chemotactic stimulation (Δche strain), the motor rotates continuously. We also showed that the chemotaxis system does not control motor speed (termed chemokinesis) as previously reported (15, 16).

By applying external force to chemotactically stopped motors, we discovered that the *R. sphaeroides* motor stops using a brake. We estimated that the motor can resist approximately 2–3 times more torque when stopped than it generates when rotating at high load. Furthermore, we found that beads are held at 27–28 discrete angles around the motor, in agreement with the 26 steps per revolution previously observed using a Na^+-driven chimeric flagellar motor in *E. coli* (17).

Results

Characterizing Motor Output. The output of the *R. sphaeroides* motor has previously been analyzed using free-swimming or tethered cells. The *R. sphaeroides* bead assay (Fig. 1*A*) was developed to improve the resolution of stop events and investigate motor speeds/torques.

Fig. 1*B* (black trace) shows a typical speed-time trace from a wild-type cell; rotation is punctuated by stop events. Beads (0.83-μm diameter) were monitored by BFP interferometry, sampled at 10 kHz and 200-point median filtered (sliding window in 1-point increments); giving a resolution of 20 ms at worst.
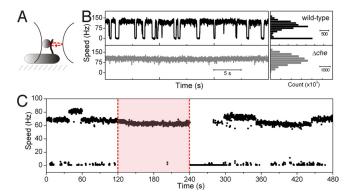
Fig. 1. Fundamental characteristics and control of the *R. sphaeroides* motor. (*A*) The bead assay was used to quantify motor output. Goat anti-rabbit IgG labeled beads were stuck to anti-flagellin rabbit IgG-labeled flagellar stubs. (*B*) A speed-time trace of a motor (0.83-μm bead) from a wild-type strain (black) and a Δ*che* strain (gray). Stable rotation, complete stops, and transient events visible in wild type are absent in the Δ*che* strain. Histograms (*right*) were constructed from speeds of all cells recorded for each strain (*n* = 41 wild type; *n* = 63 Δ*che*). The large peak at 0 Hz in the wild-type histogram, corresponding to stop events, is not present in the Δ*che* histogram. Motor speeds from the 2 strains are indistinguishable from one another. (*C*) Speed-time trace of a motor from a photoheterotrophically grown wild-type cell, recorded in a flow cell to enable buffer exchange. Speed was obtained using the power spectra of the combined *x* and *y* signals (0.83-μm bead, 1,064-nm laser, 2-kHz sampling rate). Upon addition of chemoattractant (1 mM propionate, pink shaded region) the stop frequency is reduced, but speed does not increase. Upon removal of chemoattractant, the motor stops for approximately 60 s after which the cell adapts and full-speed rotation resumes. Transient changes in speed, most likely corresponding to the association/dissociation of torque-generating units from the rotor, are clearly visible.

Three hundred seventy-six stop events from 41 cells were analyzed. The majority of transitions between run and stopped states (as defined in *Methods*) were completed in <50 ms, and there was no correlation between the time taken to decelerate/accelerate and the length of stop (Fig. S1). However, beads were often observed to rotate very slowly (≪1 Hz) during stopped states. No indication of changes in the number of stators ('de-resurrection/resurrection') going into/out of stops was observed. The mean stop length, stop frequency, and run bias (fraction of time spent rotating) were 0.66 ± 1.01 s, 0.31 ± 0.19 s^{-1}, and 0.80 ± 0.20, respectively. The run and stop intervals were found to be exponentially distributed (Fig. S2), indicating that a 2-state Markov process adequately describes the start-stop mechanism at this time resolution.

Other motor characteristics were identified. (i) Transient changes in speed were regularly observed (Fig. 1*C*, Fig. S3). These events most likely correspond to the association/dissociation of torque-generating units from the rotor as observed in *E. coli* (6). (ii) The rotational speeds of 0.83- and 1.90-μm beads (*n* = 41 and 110, respectively) were 98.6 ± 22.4 and 9.8 ± 2.9 Hz, giving torques of 1,117 ± 254 and 1,333 ± 286 pNnm/rad, respectively, similar to plateau torque values in *E. coli* (6). (iii) All of the 382 beads recorded in this study rotated in the counterclockwise (CCW) direction (as viewed from the distal end of the filament).

To determine the default motor behavior we analyzed a strain gutted of all known *che* genes (Δ*che*) and found that it rarely stops (Fig. 1*B*, gray trace). In *E. coli*, a Δ*cheA* strain is smooth swimming because CheY does not get phosphorylated (which increases the switch frequency), whereas in *B. subtilis* a Δ*cheA* strain constantly tumbles since CheY-P is required to stabilise CCW rotation. Since a Δ*cheA$_2$A$_3$* strain also exhibits smoother swimming than wild type, this indicates that the *R. sphaeroides* CheYs must stop the motor when phosphorylated.

To investigate whether *R. sphaeroides* can control motor speed and the propensity to stop, we used a flow chamber, facilitating buffer exchange. Previous experiments on photoheterotrophically grown *R. sphaeroides*, tethered in a flow chamber, suggested that rotation rates (recorded with a video camera) increase in the presence of chemoattractant (16). We repeated the experiment, this time using the bead assay. Each motor was recorded for 2 min in Hepes buffer, 2 min in chemoattractant (1 mM propionate made up in Hepes), and 4 min in Hepes. Fig. 1*C* shows a typical recording; stop frequency clearly reduces in the presence of propionate, but motor speed does not increase. When chemoattractant is removed the bead stops, usually for 1–2 min, after which periods of rotation become more and more frequent as the cell adapts. The removal of chemoattractant exaggerates what a bacterium would experience when it swims away from a chemoattractant source. Of the 26 cells recorded (10 of which were photoheterotrophically grown), the mean speed difference with and without chemoattractant was negligible (0.42 Hz).

The Motor Is 'Locked' During a Stop. To determine how CheY-P binding causes the *R. sphaeroides* motor to stop, external torque was applied to chemotactically stopped motors. CheY-P binding could cause the torque-generating units to disengage from the rotor, analogous to a clutch, or trigger the rotor to jam, analogous to a brake. To discriminate between these hypotheses we tethered cells by their flagella in a flow chamber and observed the effects of applying torque in 2 ways, using viscous flow or optical tweezers.

Viscous flow was applied continuously and a chemotactic stop induced by removal of chemoattractant. If a stop was achieved using a clutch, we expected cell bodies to orientate with the flow at 0° (Fig. 2*A*). In contrast, we found the cell body was held at particular angles irrespective of the flow direction, indicating that the motor was locked (Fig. 2*B*).

To quantify the lock torque (T_{lock}), external torque was applied using the cell body as a handle for an optical trap. The maximum torque (T_{max}) the trap can exert on the motor was calibrated against the motor's stall torque (T_{stall}) at the start of each run as described in *Methods*. T_{max} could then be varied with respect to T_{stall} by using a set of neutral density filters. After initiating a stop by removing chemoattractant, the trap attempted to move the cell body in a series of 45° angles, to a maximum of 315° (Fig. 2*C*, *Left*).

Fig. 2*C* (*Right*) shows the angle the cell body moved with the trap at various applied torques. (i) At T_{max} less than or equal to $0.2T_{stall}$, the trap was too weak to move the rotor out of the lock; after the first 45° trap increment, the cell body only moved approximately 12° and rebounded to its original position [Fig. 2*C* *Right* (*Inset*)]. (ii) At a T_{max} of $0.5–2.0T_{stall}$, the angle the rotor could be moved was variable; the cell body moved in a range from approximately 30–315°, rebounding 28 ± 14°. (iii) At a T_{max} of $3.2T_{stall}$, approximately 50% of the cells had their rotor moved until the trap was shuttered; the cell body moved with the trap up to 315°, rebounding 37 ± 18°. (iv) At a $T_{max} > 3.2T_{stall}$, the rotor could be freely manipulated with the trap; the cell body always moved all of the way to 315°, rebounding 31 ± 14° only when the trap was shuttered. Based on this, we conclude that T_{lock} is approximately $3T_{stall}$. The large variability in response at $T_{max} = 0.5–3.2T_{stall}$ may in part be attributable to the reported variation in trap stiffness at different angles (18).

The constant rebound angle ($\theta_x = 32 ± 15°$) indicates that a torque (T_x), was maintained throughout the forced rotation of the locked motor. T_x was compared with T_{lock} as follows. The *R. sphaeroides* tether relaxes exponentially (Fig. S4) with a time constant τ. We therefore calculated tether stiffness (κ_θ) using (i) the equipartition method ($n_{cells} = 33$) and (ii) $\tau = f/\kappa_\theta$ where f is the drag coefficient of the tethered cell (as described in *Methods*, $n_{cells} = 5$). This gives $\kappa_\theta = 3,200 ± 2,000$ and $4,500 ±$
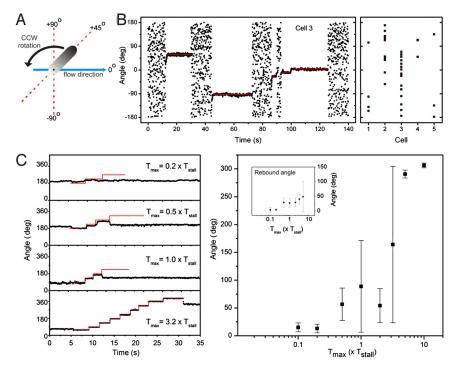
Fig. 2. Application of external torque to the *R. sphaeroides* motor during a stop. Long stops were induced by removing chemoattractant as in Fig. 1C. (*A*) External torque was applied by continuously flowing buffer at a constant rate. For positive angles the cell body rotates against the flow, negative angles with the flow. Clutch induced stops would cause the cell body to orientate with the flow at 0°. (*B*) Angle-time trace showing stops at random angles. The stop at −90°, most clearly shows the presence of a lock. At this position the cell body was rotating with the flow, therefore there is no possibility that the motor stopped because it is stalled by the flow (rather than chemotactically stopped). (*B, Right*) The stop angles of another 4 cells also occurred at random. (*C*) External torque was applied using an optical trap. (*Left*) Angle-time traces of tethered cells as above (black), with the angle of the trap when on (red). During a long chemotactic stop the trap attempted to move the cell forward in 45° increments, up to a maximum of 315°. With a weak trap ($T_{max} = 0.2 \times T_{stall}$) the cell body did not follow the trap; intermediate traps ($T_{max} = 0.5$ or $1.0 \times T_{stall}$) held the cell for several increments before escaping; the stronger traps ($T_{max} = 3.2 \times T_{stall}$) held the cell all of the way to 315° (see Movie S1). (*C, right*) Mean angle cell bodies moved as a function of trap strength (T_{max}) for the dataset; $n_{runs}(n_{cells}) = 6$ (4), 4 (4), 7 (5), 9 (7), 6 (4), 10 (9), 4 (4), and 2 (2). At $3.2 \times T_{stall}$ external torque was large enough to force the rotor out of the locked state in 50% of cases. The *inset* shows the mean cell body rebound angle upon release/escape from the trap. For $T_{max} < 0.2 \times T_{stall}$ cells rebounded to their starting point. For $T_{max} > 0.2 \times T_{stall}$ cells rebounded approximately 30°.

2,000 pNnm/rad² and thus $T_x = \kappa_\theta \cdot \theta_x = 1,700 \pm 900$ and $2,600 \pm 500$ pNnm/rad for the 2 methods, respectively. Given that T_{stall} is approximately 1,225 pNnm/rad (plateau torque obtained earlier), T_x is approximately $2T_{stall}$ in broad agreement with the results above ($T_{lock} \approx 3T_{stall}$).

The Motor Stops at Discrete Angles. To gain more information about the motor-locking mechanism, angle-time traces of beads on flagellar stubs of wild-type cells were examined. Fig. 3 shows that beads are held at particular angles, showing no large-scale Brownian motion during a stop. These angles are maintained for extensive periods of time when stops are induced by removing chemoattractant (Fig. 3B). Beads (0.83-μm) attached to filament stubs of free motors would be expected to move approximately 172° in 2 s (root mean square angular deviation) by free rotational Brownian motion alone. It is also apparent that beads can advance in a series of steps in angle during periods of slow rotation.

To increase the chance of observing steps, $CheY_6$ was over-expressed (in a wild-type background, WT+CheY6, Table S1) from pIND4, resulting in an increase in stop frequency. Under these conditions, the motor regularly underwent prolonged stop events with 'steppy' slow rotation. Fig. 4 *A* and *B* show examples of steppy traces observed from wild-type and WT+CheY6 cells. Backwards steps were not observed. The data were subjected to step analysis as described in ref. 17. Fig. 4*C* shows the step size histogram for the clearest steps in the dataset. A Gaussian fit gives a peak of $13.0 \pm 4.5°$ corresponding to approximately 27–28 steps per revolution.

Discussion

We were able to accurately access *R. sphaeroides* motor output by monitoring the rotation of beads on flagellar stubs. Signal inputs to the motor were manipulated, either genetically or by exposing cells to different chemotactic stimuli. We found that

Fig. 3. Beads are held at constant angles during a stop. Angle of beads (0.83-μm) attached to flagellar stubs from wild-type cells as a function of time. Traces were obtained using a 632-nm laser (10-kHz sampling rate) and a 1,064-nm laser (2-kHz sampling rate) for *A* and *B*, respectively. Beads are held at constant angles and show no large-scale Brownian motion during a stop at steady-state (*A*) or when long chemotactic stops are induced by removal of chemoattractant (*B*). (*B, inset*) shows the bead rotating very slowly forward in a series of steps during stop events.

Fig. 4. Step analysis. (*A*) Examples of angle-time traces showing steps during stop events from wild-type (blue) and WT+CheY6 (black) cells. Wild-type data were obtained with either a 632-nm laser (10-kHz sampling rate) or a 1,064-nm laser (2-kHz sampling rate); WT+CheY6 motors were recorded with a 1,064-nm laser at 5-kHz sampling rate (in all cases 0.83-μm beads were used). The output of a step-finding algorithm is superimposed (red). (*B*) A particularly clear steppy angle-time trace an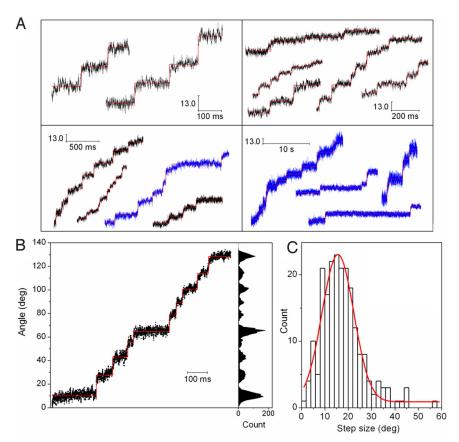d its accompanying histogram of dwell angles (bin size = 1°). (*C*) The histogram of step sizes obtained by the step-finding algorithm (n_{steps} = 5,361; histogram bin size = 2°). The peak (Gaussian fit) at 13.0 ± 4.5° corresponds to approximately 27–28 steps per revolution.

the motor rotates continuously in the CCW direction unless signaled to stop via phosphorylated CheYs. Only the motor stop frequency, and not its speed, is controlled by the chemotaxis system. Stops began and ended within approximately 50 ms, close to the resolution time of our measurements using the bead assay ($\approx$20 ms). If the motor were to lock instantaneously, the tether would relax exponentially from an initial twist angle $\theta = T/\kappa_\theta$, to $\theta = 0$, with a time constant $\tau = f/\kappa_\theta$; where T is the motor torque, f the drag coefficient and κ_θ the tether stiffness. The initial speed of this relaxation would be $\omega = \kappa_\theta \cdot \theta/f = T/f$, the same as the speed at which the motor was running. With our estimates of T, f, and κ_θ we obtain $\theta = 16 \pm 8°$, with time constants $\tau = 0.4 \pm 0.2$ and 190 ± 80 ms for 0.83-μm beads and tethered cells, respectively. Thus, slow forward rotation at the beginning of some stops in tethered cell traces could be explained by tether relaxation, but in most cases, the movement is larger than 16° and slower than 190 ms. Tether relaxation cannot explain the observation of slow ($\ll$1 Hz) steppy forward rotation lasting several seconds in 0.83-μm bead traces (Fig. 3).

By applying external torque to the motor using 2 independent techniques, we found that during chemotactic-induced stops, motors resisted rotation indicating a braking mechanism. Using the cell body as a handle for an optical trap we estimated that the brake can resist a torque up to 2–3 times the stall torque of the motor. In contrast, recently Blair et al. showed that *Bacillus subtilis* uses a molecular clutch to disable its flagella during biofilm formation (19). Tethered cells overexpressing the clutch-initiating protein, EspE, behaved as although they were unpowered, analogous to a strain lacking torque-generating units

($\Delta motAmotB$). The difference may reflect requirements for long-term stopping during biofilm formation versus fast reversible control needed for chemotaxis.

Consistent with a brake mechanism, beads attached to flagellar stubs remain at a fixed angle for several seconds during stops, exhibiting only small fluctuations (significantly smaller than the step size of $\approx$13°). Some motors showed slow stepping rotation during stops, stopping at 27–28 discrete angles around the motor. This is in agreement with the approximately 26 steps per revolution observed previously using a Na$^+$-driven chimeric flagellar motor in *E. coli*, measured at low sodium-motive force and with controlled expression of a small number of torque-generating units (17).

In bidirectional motors, the binding of CheY-P to the switch complex is presumed to instigate a conformational change in FliM, which in turn affects the orientation of the charged ridge in the C terminus of FliG (20, 21). The different electrostatic interactions resulting from this altered rotor-stator interface [between FliG and the cytoplasmic loop of the stator (MotA)], are thought to be responsible for rotation in the alternative direction (22).

Similarly, this altered rotor-stator interface may stop the *R. sphaeroides* motor: Conformational changes during a stop must lock the motor, either in 1 of the states through which it normally cycles during torque generation or in a state that is only present during a chemotactic stop. In either case, the observed steps in angle could be due either to rapid transitions between the stopped and cycling states or to a temporary reduction in the amplitude of the locking potential that permits a thermally

BIOPHYSICS AND COMPUTATIONAL BIOLOGY

activated jump from 1 minimum to the next. The exaggerated stepping behavior of a strain overexpressing $CheY_6$, which can bind in a phosphorylated or unphosphorylated state (23) is compatible with both stepping mechanisms.

The similar periodicity of steps observed in chemotactically stopped *R. sphaeroides* motors with a full complement of stators and in chimeric motors with few stators present (17), indicates that the step size is governed solely by the periodicity of the rotor ring. The locked state is described by an interaction potential between the rotor and each stator, and these potentials will each share the approximately 27-fold periodicity of the rotor. Thus, the rotor will step in a combined potential that is the sum of the individual rotor-stator potentials. The amplitude of the combined potential depends upon both the number and relative phase of the individual potentials, which might in part account for the observed variability in the locking strength at $T_{max} = 0.5–3.2T_{stall}$. However, the periodicity of the combined potential stays the same irrespective of the number and relative phase of the individual potentials, which might explain why step size is independent of the number of stators, as observed. If the step size is found to be independent of the number of stators in a running motor and in the locked motors observed in this study, an alternative explanation could be that the stators are separated by angles close to an integer multiple of the rotor periodicity (24).

At this stage, the potentials discussed above are hypothetical. In practice they are likely to be because of interactions between the charged residues that have been shown to affect motor function in *E. coli* (K264, R281, D288, D289, and R297 in FliG, and R90 and E98 in MotA) (4), all of which are conserved in *R. sphaeroides*. Analysis of strains harboring point mutations at these sites may reveal details of the locking mechanism.

Our estimated tether stiffness ($\kappa_\theta = 3,800 \pm 2000$ pNnm/rad^2) is an order of magnitude higher than that of *E. coli*, which was attributed primarily to flexibility of the hook (25, 26). This is consistent with electron micrographs showing that the *R. sphaeroides* hook is straight, not curved like *E. coli* (27). Recent models of the flagellar motor have proposed elastic links between stators and the cell wall, each with a stiffness of approximately 200 pNnm/rad^2 (24, 28). Approximately 11 such stators in parallel (6) would have a combined stiffness within the range of our estimates for the *R. sphaeroides* tether, but $\approx$10 times stiffer than the *E. coli* tether. Thus, it is possible that the *R. sphaeroides* hook is stiffer than or comparable to the stator springs, and that the latter dominate the tether stiffness. In this case, variation in the number of stators would contribute to variability in tether stiffness. However, until direct evidence is obtained for the existence of compliant stator springs these considerations remain speculative.

High-resolution measurements of rotating beads coupled with the application of external torque have revealed how the *R. sphaeroides* flagellar motor is stopped. This provides an insight into how nature uses fundamental mechanical principles to operate motors effectively at the nanoscale.

Methods

Strains. *R. sphaeroides* strains (Table S1) were grown from frozen stocks (made from single colonies) in succinate medium (29) at 30 °C to an OD of 0.45–0.65, either aerobically with shaking without illumination, or when specified, photo-heterotrophically in an anaerobic cabinet with illumination at 50 μmol/m^2/s. Media were supplemented with 25 μg/mL kanamycin and 1 mM IPTG (overnight induction) when using pIND4. Although the *R. sphaeroides* genome encodes 2 sets of *fla* genes (30), only the fla1 set has ever been observed under these conditions.

Bead and Tethered Cell Assay. Carboxy-modified latex spheres (4% wt/vol, Interfacial Dynamics Corp.) were covalently coupled to goat anti-rabbit IgG (Abcam) in 50 mM Mes (pH 6) plus 50 mg/mL EDAC (Invitrogen). Cells with truncated filaments were immobilized to the glass surface via polylysine (17). The filament stubs were coated with anti-flagellin rabbit IgG for attachment to antibody labeled beads. In the tethered cell assay, cells were immobilized to the coverslip via anti-flagellin antibody as described in ref. 13. All experiments were performed in 10 mM Na-Hepes, pH 7.2, except where stated, when Hepes was supplemented with 1 mM sodium propionate (Sigma).

Speed, Stopping, and Running Torque Measurements. The position of rotating beads was detected by BFP interferometry (31) using a 632 nm Helium Neon or 1,064 nm Ytterbium fibre laser (18). All experiments were performed at 23 °C.

Bead angle was computed as described in ref. 17. Speeds were calculated from angle versus time traces ($d\theta/dt$) and filtered with a 200-point median filter (sliding window in 1-point increments), or where stated, by means of power spectra of the combined x and y signals (31).

For Fig. 1B, cells were selected as follows. (i) The mean speed (M_{CCW}) for each record was calculated by fitting a Gaussian to the peak in the speed histogram corresponding to intervals during which the bead was spinning. (ii) Stop events were measured from when speed decreased to $0.1\,M_{CCW}$ to when speed increased $>0.4\,M_{CCW}$. (iii) Stop events were screened by a 45° moving window and the largest number of stops registered within a 45° sector subjected to a binomial test. Cells with nonuniformly distributed stop angles were discarded.

Deceleration times were defined as the time it takes for the speed of the bead attached to the filament stub to decrease from 0.7 M_{CCW} to 0.1 M_{CCW} (or from 0.1 M_{CCW} to 0.7 M_{CCW} for acceleration times).

Torque ($T = f2\pi M_{CCW}$) was estimated by calculating the viscous drag (f) on the bead, $f = 8\,\pi\eta r^3 + 6\,\pi\eta r l^2$ where η is viscosity, r is bead radius, and l is eccentricity. For the bead sizes used, contribution from the filament stub is negligible and was therefore neglected (32). The eccentricity of rotation was 126 ± 28 and 299 ± 91 nm for 0.83-μm and 1.90-μm beads, respectively, measured as described previously in refs. 6, 18.

Lock Torque Measurements. The trap and rotating tethered cells were aligned as previously described (18). T_{max} was calibrated against T_{stall} at the start of each run while keeping the trap at a fixed position, until the rotating cell body was just stalled. The laser was shuttered and a chemotactic stop induced by removal of chemoattractant. The shutter was opened and the trap used to move the cell body in a series of 45° angles (up to a maximum of 315°). The trap was once again shuttered and the motors allowed to resume rotation. The procedure was repeated with different values of T_{max}: (0.1, 0.2, 0.5, 1.0, 2.0, 3.2, 5.0, and 10.0) $\times$ T_{stall}. The position of the cell body was recorded using a video camera (LCL-902K, Watec) at 50 Hz. Cells were rejected if they appeared to be sticking or took longer than 2 min (the maximum recovery time without mechanical manipulation) to recover. At $T_{max} = 10T_{stall}$, some motors appeared to break permanently (no recovery within 12 min), similar to when the *E. coli* motor is driven backwards (33).

For T_x calculation, we confirmed that the *R. sphaeroides* tether behaves like a linear spring, validating the use of the equipartition method ($\kappa_\theta < \Delta\theta^2 > = k_B T$) to estimate κ_θ directly. In addition, κ_θ was estimated by fitting the relaxation angle of the cell body with an exponential of time constant (τ), where $\tau = f/\kappa_\theta$ (f being the drag coefficient of the tethered cell). f of each individual cell was calculated from the speed of the cell's rotation before and after external torque was applied. It was not possible to accurately estimate the rebound angle at $T_{max} = 10T_{stall}$ because at such large torques, the cell body moved from its initial centre of attachment, introducing a large error.

Steps. Step analysis was performed using a computer algorithm as described in ref. 17. In theory the peak value of 'quality factor' (as a function of the ratio of the length of the data trace and number of steps fitted) gives a fit that best represents real steps in the data (34). In practice a fit that slightly overfits the data (but still gives a high 'quality factor') was chosen (34, 17).

1. van den Heuvel MGL, Dekker C (2007) Motor proteins at work for nanotechnology. *Science* 317:333–336.
2. Berg HC (2003) The rotary motor of bacterial flagella. *Annu Rev Biochem* 72:19–54.
3. Sowa Y, Berry RM (2008) Bacterial flagellar motor. *Quart Rev Biophys* 41:103–132.
4. Zhou J, Lloyd SA, Blair DF (1998) Electrostatic interactions between rotor and stator in the bacterial flagellar motor. *Proc Natl Acad Sci USA* 95:6436–6441.
5. Leake MC, et al. (2006) Stoichiometry and turnover in single, functioning membrane protein complexes. *Nature* 443:355–358.

6. Reid SW, et al. (2006) The maximum number of torque-generating units in the flagellar motor of *Escherichia coli* is at least 11. *Proc Natl Acad Sci USA* 103:8066–8071.

7. Wadhams GH, Armitage JP (2004) Making sense of it all: Bacterial chemotaxis. *Nat Rev Mol Cell Biol* 5:1024–1037.

8. Hazelbauer GL, Falke JJ, Parkinson JS (2008) Bacterial chemoreceptors: High-performance signaling in networked arrays. *Trends Biochem Sci* 33:9–19.

9. Cluzel P, Surette M, Leibler S (2000) An ultrasensitive bacterial motor revealed by monitoring signaling proteins in single cells. *Science* 287:1652–1655.

10. Darnton NC, Turner L, Rojevsky S, Berg HC (2007) On torque and tumbling in swimming *Escherichia coli*. *J Bacteriol* 189:1756–1764.

11. Porter SL, Wadhams GH, Armitage JP (2008) Rhodobacter sphaeroides: Complexity in chemotactic signalling. *Trends Microbiol* 16:251–260.

12. Porter SL, et al. (2006) The CheYs of *Rhodobacter sphaeroides. J Biol Chem* 281:32694–32704.

13. Armitage JP, Macnab RM (1987) Unidirectional, intermittent rotation of the flagellum of *Rhodobacter sphaeroides. J Bacteriol* 169:514–518.

14. Armitage JP, Pitta TP, Vigeant MA, Packer HL, Ford RM (1999) Transformations in flagellar structure of *Rhodobacter sphaeroides* and possible relationship to changes in swimming speed. *J Bacteriol* 181:4825–4833.

15. Brown S, Poole PS, Jeziorska W, Armitage JP (1993) Chemokinesis in *Rhodobacter sphaeroides* is the result of a long term increase in the rate of flagellar rotation. *Biochim biophys Acta* 1141:309–312.

16. Packer HL, Lawther H, Armitage JP (1997) The *Rhodobacter sphaeroides* flagellar motor is a variable speed motor. *FEBS Lett* 409:37–40.

17. Sowa Y, et al. (2005) Direct observation of steps in rotation of the bacterial flagellar motor. *Nature* 437:916–919.

18. Pilizota T, et al. (2007) A programmable optical angle clamp for rotary molecular motors. *Biophys J* 93:264–275.

19. Blair KM, Turner L, Winkelman JT, Berg HC, Kearns DB (2008) A molecular clutch disables flagella in the *Bacillus subtilis* biofilm. *Science* 320:1636–1638.

20. Brown PN, Terrazas M, Paul K, Blair DF (2007) Mutational analysis of the flagellar protein FliG: Sites of interaction with FliM and implications for organization of the switch complex. *J Bacteriol* 189:305–312.

21. Passmore SE, Meas R, Marykwas DL (2008) Analysis of the FliM/FliG motor protein interaction by two-hybrid mutation suppression analysis. *Microbiology* 154:714–724.

22. Van Way SM, Millas SG, Lee AH, Manson MD (2004) Rusty, jammed, and well-oiled hinges: Mutations affecting the interdomain region of FliG, a rotor element of the *Escherichia coli* flagellar motor. *J Bacteriol* 186:3173–3181.

23. Ferre A, de la Mora J, Ballado T, Camarena L, Dreyfus G (2004) Biochemical study of multiple CheY response regulators of the chemotactic pathway of *Rhodobacter sphaeroides. J Bacteriol* 186:5172–5177.

24. Bai F, Lo C-J, Berry RM, Xing J (2009) Model studies of the dynamics of bacterial flagellar motors. *Biophys J* 96:3154–3167.

25. Block SM, Blair DF, Berg HC (1989) Compliance of bacterial flagella measured with optical tweezers. *Nature* 338:514–518.

26. Block SM, Blair DF, Berg HC (1991) Compliance of bacterial polyhooks measured with optical tweezers. *Cytometry* 12:492–496.

27. Ballado T, Camarena L, González-Pedrajo B, Silva-Herzog E, Dreyfus G (2001) The hook gene (*flgE*) is expressed from the *flgBCDEF* operon in *Rhodobacter sphaeroides*: Study of an *flgE* mutant. *J Bact* 183:1680–1687.

28. Yuan J, Berg HC (2008) Resurrection of the flagellar rotary motor near zero load. *Proc Natl Acad Sci USA* 105:1182–1185.

29. Sistrom WR (1960) A requirement for sodium in the growth of *Rhodopseudomonas spheroides. J Gen Microbiol* 22:778–785.

30. Poggio S, et al. (2007) A complete set of flagellar genes acquired by horizontal transfer coexists with the endogenous flagellar system in *Rhodobacter sphaeroides. J Bacteriol* 189:3208–3216.

31. Ryu WS, Berry RM, Berg HC (2000) Torque-generating units of the flagellar motor of *Escherichia coli* have a high duty ratio. *Nature* 403:444–447.

32. Inoue Y, et al. (2007) Torque-speed relationships of Na$^+$-driven chimeric flagellar motors in *Escherichia coli. J Mol Biol* 376:1251–1259.

33. Berg HC, Turner L (1993) Torque generated by the flagellar motor of. *Escherichia coli. Biophys J* 65:2201–2216.

34. Kerssemakers JWJ, et al. (2006) Assembly dynamics of microtubules at molecular resolution. *Nature* 442:709–712.

BIOPHYSICS AND COMPUTATIONAL BIOLOGY